A first-order evaluation of climate outlooks based on the IPCC A2 and B2 SRES emission scenarios.

By R.E. Benestad

The Norwegian Meteorological Institute, PO Box 43, 0313, Oslo, Norway *

1st DRAFT (REB) January 28, 2003

ABSTRACT

The output from transient simulations of temperature and precipitation from 8 different climate model derived using the IPCC SRES emission scenarios A2 and B2 as boundary conditions was examined. The climate model data was converted from the GRIB format to netCDF and subject to a simple analysis. An ensemble was constructed from the results of different models. A first-order evaluation of the geographical distribution of the mean climatic elements suggests a high degree of realism in the model scenarios.

An analysis was carried out examining the ensemble mean and the spread. Furthermore, the dependency of estimated trend to the altitude, distance from the coast, and latitude was investigated. A comparison between temperature trends suggest most rapid warming in the high northern latitudes and strongest precipitation trends in the tropics.

KEY WORDS: Climate change   Climate model evaluation   Trend analysis   Multi-model ensemble.

* *Corresponding author: R.E. Benestad, rasmus.benestad@met.no, The Norwegian Meteorological Institute, PO Box 43, 0313 Oslo, Norway, phone +47-22 96 31 70, fax +47-22 96 30 50*

Model	Flux adj.	ny × nx	
		TABLE 1.	
CCCma	Yes	96 × 48	Canada
CCSR/NIES	Yes	64 × 32	Japan
CSIRO Mk2	Yes	64 ×56	Australia
ECHAM4/OPYC3	Yes	128 × 64	Germany
GFDL-30	No	96 × 80	U.S.A.
GFDL-30 (SLP)		192 × 80	
HadCM3	No	96 × 73	U.K.
NCAR-CSM	No	128 × 64	U.S.A.
NCAR-PCM	No	128 × 64	U.S.A.

1   Introduction

It is important to apply a quality control to climate model (coupled Atmosphere Ocean General Circulation Model, AOGCM) data before using these to derive downscaled climate scenarios. A conversion of data formats should always be accompanied with a first-order quality control to make sure that the coordinates and time stamp are correct and that the values have not been corrupted. It is also important to check whether the output from the climate models give a realistic description of the actual climate.

2   Methods & Data

The climate scenarios were retrieved from the IPCC GCM data gate way (ftp://info.dkrz.de/pub/cera) and converted from the GRIB format to ASCII using `dkrz_readgrib` (a C++ code from IPCC) and from ASCII to netCDF using `asc2ncdf` (A FORTRAN code written by R.E. Benestad). The data format conversion was similar to *Benestad* (2000), and the R-package `clim.pact`[†] was used for the analysis. Only the IPCC B2 ("Global sustainability" story line) and A2 ("'World Markets' story line) SRES scenarios are discussed here.

The latitude coordinates in the for instance NCAR-PCM and CCCma data were accidentally reversed, and in order to fix this problem, the latitude values are given in units "degrees-south" (`clim.pact` handles these units). A few small errors from the conversion were corrected by altering appropriate attributes in the file headers using the FORTRAN scripts `fix_torg` (set the correct time origin so the time stamp is right), `fix_scal` (in some files, the actual data values were stored as "Pa" whereas the unit in the header said "hPa", the script changes the unit in the header to "Pa"), and `fix_lats` (Changes the latitude units from "degrees-north" to "degrees-south"). The retrieval and reformatting for the sea level pressure (SLP) for the GFDL models were unsuccessful, and hence the SLP from the GFDL models is not included here.

The first-order data control described in this report consists of maps of the mean values for the interval "2000"–"2049". A distinction will be made in this report between the actual time and the model date by expressing the model dates in apostrophes. Thus, the year 1990 means the real date with which historical observations may be associated, whereas the model year "1990" denotes a year in the model simulations which is meant to describe a model climate analogous to the actual 1990 climate. Since the "2000"–"2049" represents the "future", the evaluation of the mean field will not entail a direct comparison with the observations, but merely give an indication of whether these means are realistic or whether these are very different from the present climatic state. The evaluation will mainly consist of a comparison between the various model output.

Warming trends were derived by regressing (least squares fit) the grid-box values against a linear model for "2000"–"2049" (For the NCAR-CSM, "2010"–"2059" was used due to unrealistically low initial temperatures), and the warming rate was taken as the slope of the best-fit. The warming rate was then examined in terms of altitude, latitude and distance-from-the-coast dependencies. All the model scenarios were re-gridded to a 2.5 × 2.5° by bivariate linear interpolation. The altitudes for each grid-box was estimated for the 2.5 × 2.5° grid by applying a similar interpolation to a 60-minute resolution topography (shown in Figures 14b & fig:14b). The distance from the coast was (crudely) estimated in terms of degrees, by taking the minimum value derived from the coordinates of the coasts and the

[†]Version 1.0, which is based on the earlier version *Benestad* (2003).

coordinate of the respective grid-box. This estimate results in a latitudinal bias, with distances in the polar regions being over-estimated.

3 Results

3.1 A quality control of the mean fields

In order to make a judgment about whether the climate simulations are realistic or not, one may look to the actual state of the climate system. Here, the reanalyses from the National Center for Environmental Predication (NCEP) in the U.S.A, henceforth referred to as the NCEP reanalysis *Kalnay* et al. (1996) will be used as a description of the present climate. However, it is important to keep in mind that the reanalysis does not give a perfect description of the real climate system. The NCEP reanalysis values for precipitation, specific humidity and snow are derived through the means of a numerical weather model (NWM), and are subject to the ability of this model to give a true reproduction of the actual values. Since these are model derived, they are associated with a high degree of uncertainty.

Figure 1 shows the geographical distribution of a selection of climate elements according to the NCEP reanalysis. The temperature is generally higher in the tropics and near the sea level and lower near the poles and in high-altitude regions such as the Himalayas and the Andes (a). The regions with the most precipitation are the Inter-Tropical Convergence Zone (ITCZ), South Pacific Convergence Zone (SPCZ), and over Indonesia and central Africa (b). The precipitation is higher in the northern ITCZ than in the souther ITCZ. It is important to keep in mind the fact that these values are mostly model predictions. For SLP, there are well-known features as the Azores, southeast Pacific, south Atlantic and south Indian sea highs and Aleutian and Icelandic lows (c). The most pronounced feature is nevertheless the zonal band of low SLP over the Southern Sea and high SLP over parts of the Antarctic. The latter high pressure region may is subject to high uncertainties due to few observations from this remote and hostile part of the world. The 850hPa temperature (d) exhibits similar large-scale features as the near-surface air temperature (a), but with a greater land-sea contrast: warmer over land. Panel (e) shows the specific humidity q which generally indicates a high level of moisture in the topics. There is surprisingly high values for q near the Himalayas, and the question whether these are due to the south Asian Monsoon or due to model errors is outside the scope of this report. The snow-cover in panel (f) shows an expected distribution with more extensive cover in the high latitudes.

Figure 2 shows a comparison between the unadjusted global mean temperature derived from the various climate models following the IPCC B2 (a) and A2 (b) SRES emission scenarios. These curves are comparable to the (*Houghton* et al., 2001, Figure 9.6, p. 542) results, but not exactly identical due to different type of preprocessing and filtering. All the different models show similar trends, albeit at a different temperature "level". The NCAR-PCM model systematically predicts lower temperatures than the others. Furthermore, the initial temperatures in the NCAR-PCM data file were set to unrealistically low values (an initial step is seen in the figure), and this initial jump in the data caused some problems in the initial trend analysis (too large trends). By applying the trend analysis to a slightly shifted time interval for this model ("2010"–"2059"), the trends were in much better agreement with the other models (see below).

Figure 3 shows a comparison between the various global mean precipitation scenarios in terms of mm/day. There is a fair agreement amongst the various models on the mean value, and they tend to agree on a weak positive trend. The trends shown here seem less dramatic than those seen in (*Houghton* et al., 2001, Figure 9.6, p. 542), however, the latter shows the precipitation in terms of change in %. According to Figure 3 NCAR-CM predicts a wetter world than the other models.

On a smaller scale, the model scenarios show less agreement, although the inter-model agreement is still fairly good. Figure 4 shows the spatial mean temperature estimated for the region 40°W–40°E, 45°N–85°N which covers most of Europe and the Greenland-Iceland-Norwegian-Barents Seas. The models (CCSR/NIES) giving the highest global mean temperature also produces the highest values near Europe in the B2 scenario. In the A2 scenario, on the other hand, it is the ECHAM4/OPYC3 model that predict the highest temperatures, both in the global and 40°W–40°E, 45°N–85°N mean.

The projected mean precipitation trends over 40°W–40°E, 45°N–85°N are similar in the various model scenarios, although two models (ECHAM4/OPYC3 and NCAR-PCM) give mean precipitation that are systematically higher than the other models (Figure 5a–b). The models suggest a weak trend
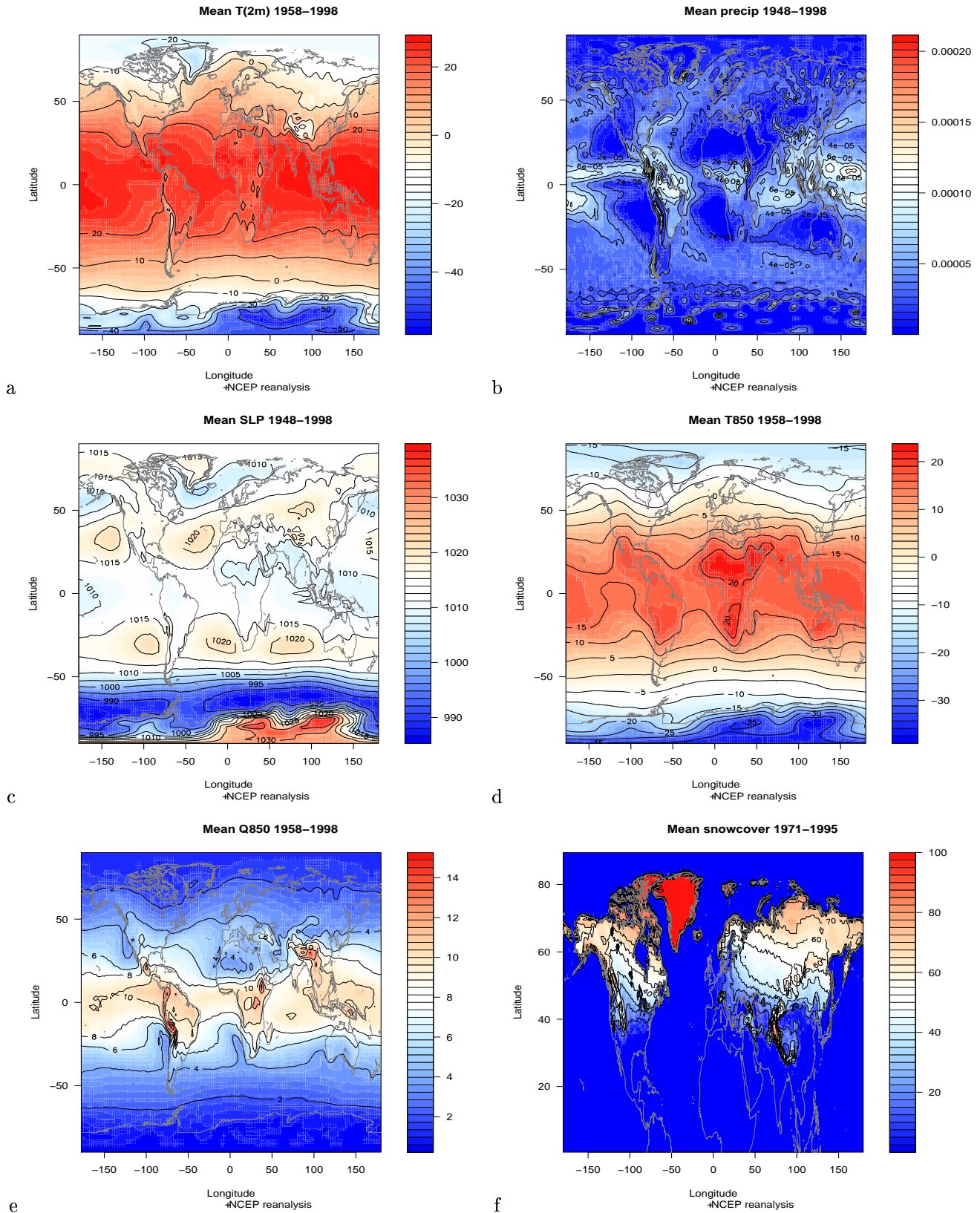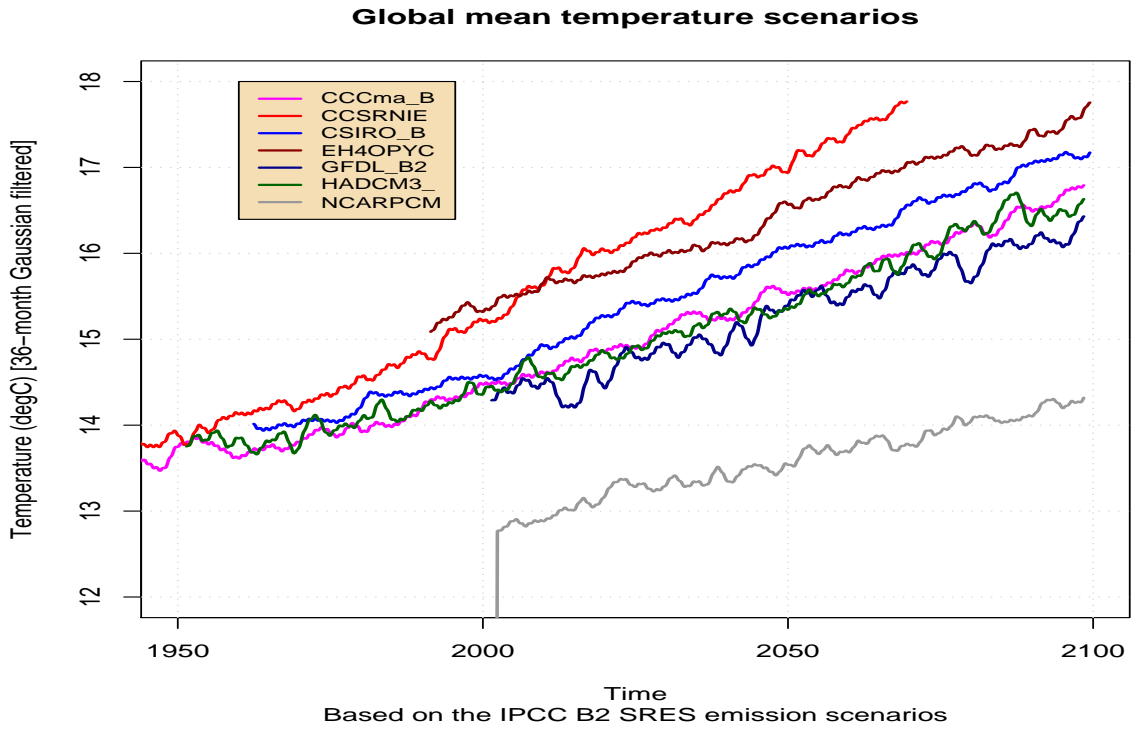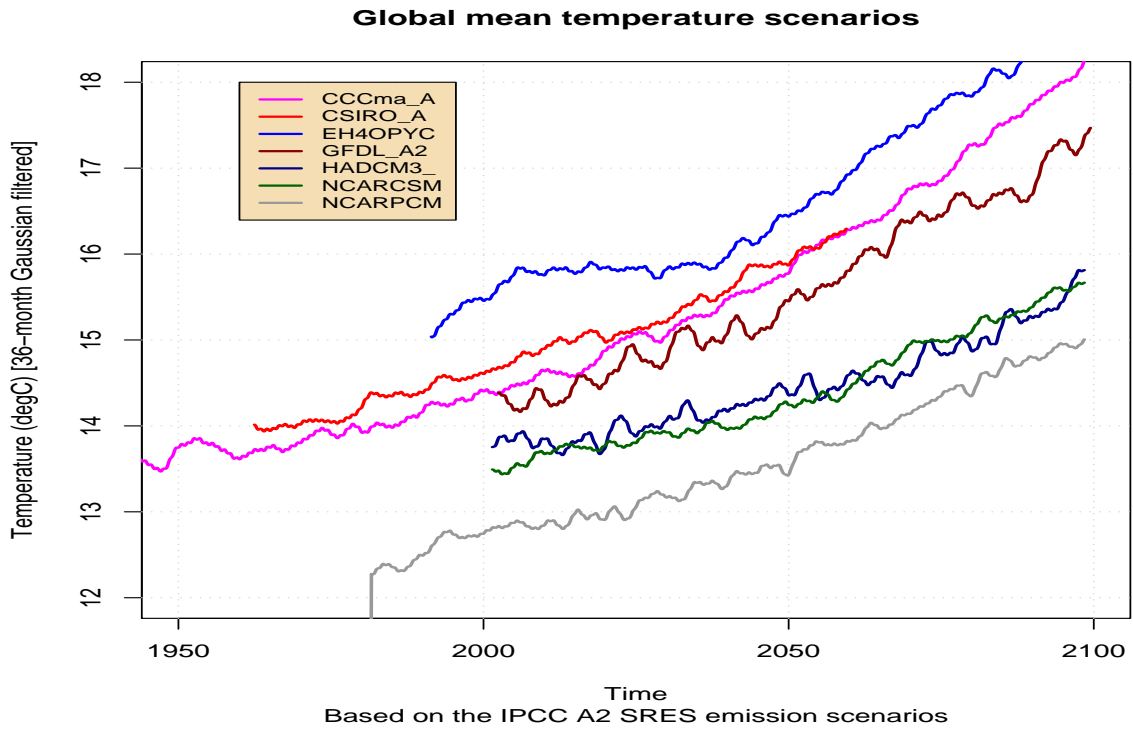
Figure 1.   Maps showing the geographical distribution of mean values for a) T(2m), b) precipitation (in units of $Kg/m^2/s$), c) SLP, d) T(850hPa), e) specific humidity at 850hPa, and the snow-cover (all seasons). Note: the snow data is only shown for the Northern Hemisphere.
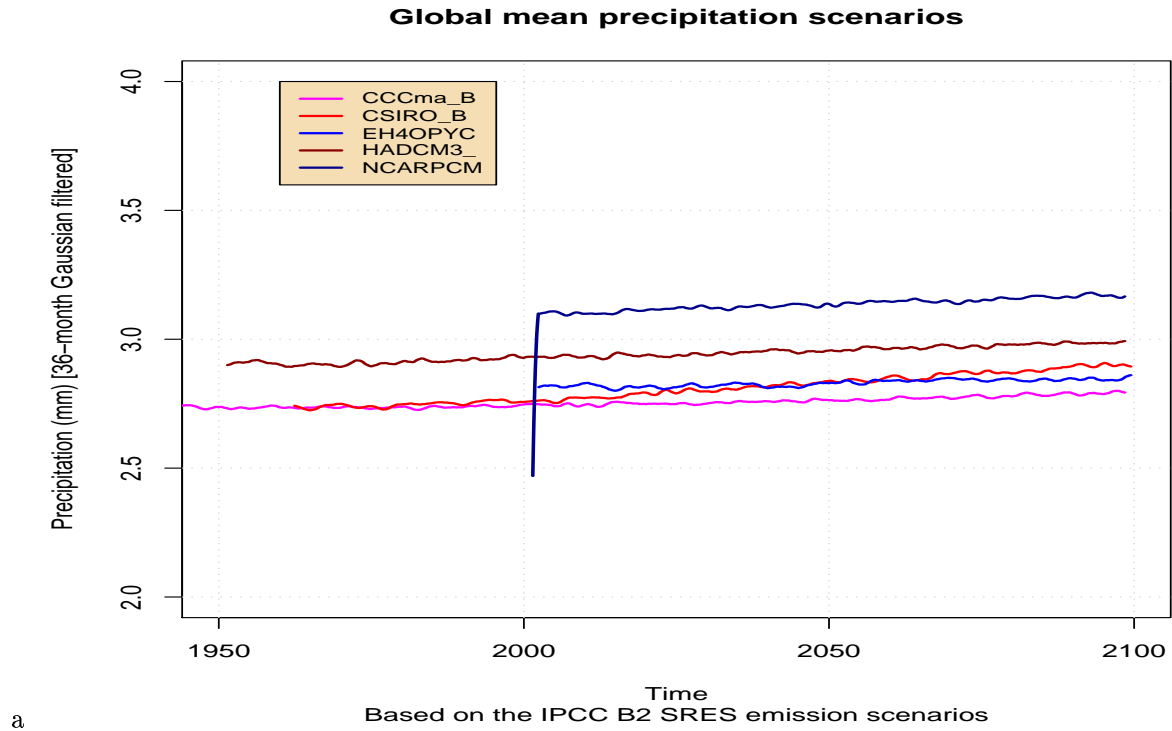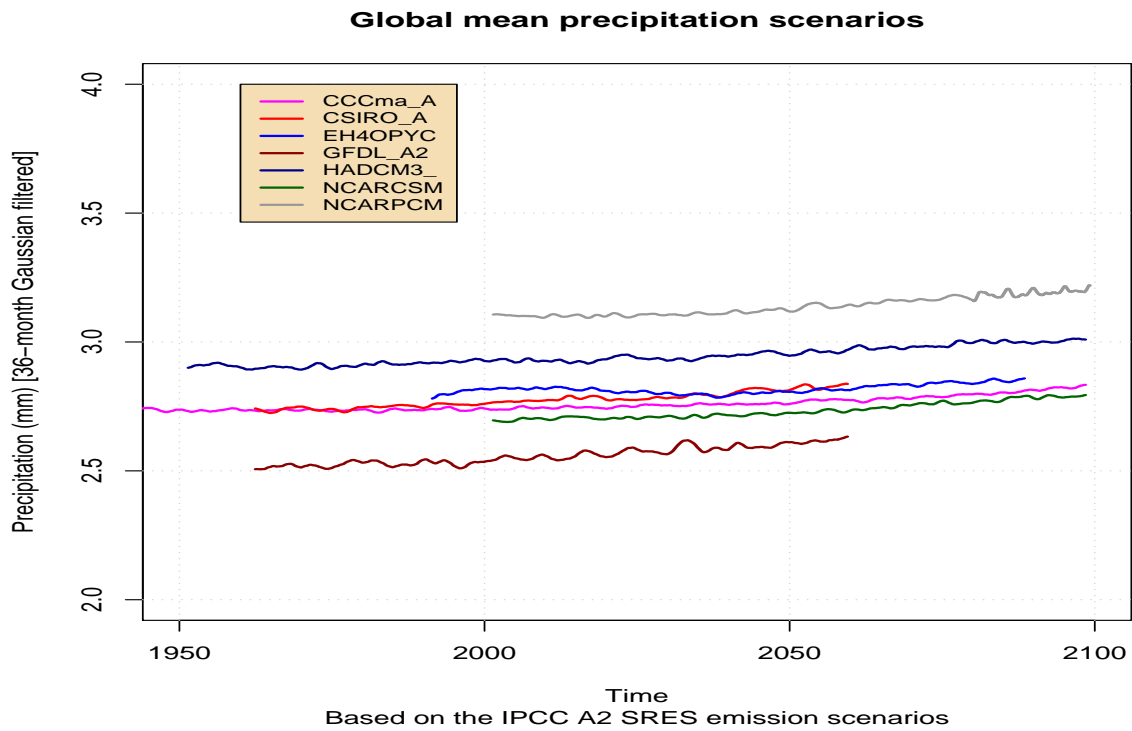
Global mean temperature scenarios

a
Based on the IPCC B2 SRES emission scenarios

Global mean temperature scenarios

b
Based on the IPCC A2 SRES emission scenarios

Figure 2. Comparison of the the global mean temperature computed by climate models following the IPCC a) B2 and b) A2 SRES scenarios.

Global mean precipitation scenarios

a

Global mean precipitation scenarios

b

Figure 3. Comparison of the the global mean precipitation computed by climate models following the IPCC a) B2 and b) A2 SRES scenarios.

North Atlantic mean temperature scenarios

a

Based on the IPCC B2 SRES emission scenarios

North Atlantic mean temperature scenarios

b

Based on the IPCC A2 SRES emission scenarios
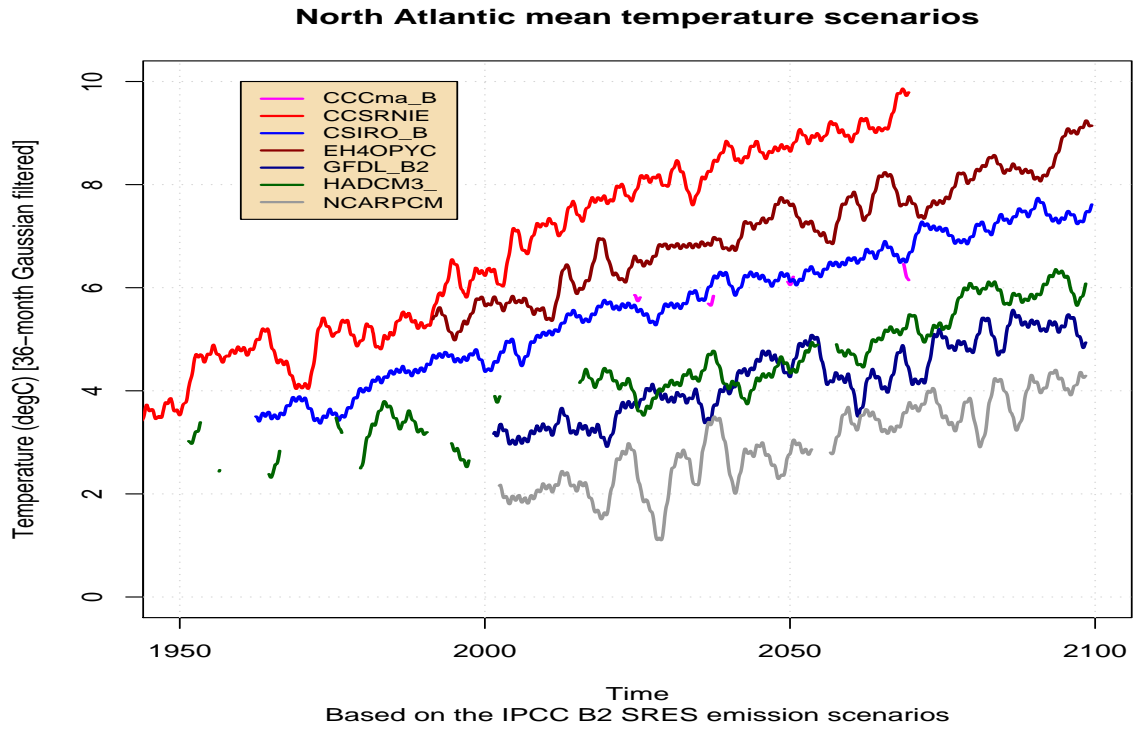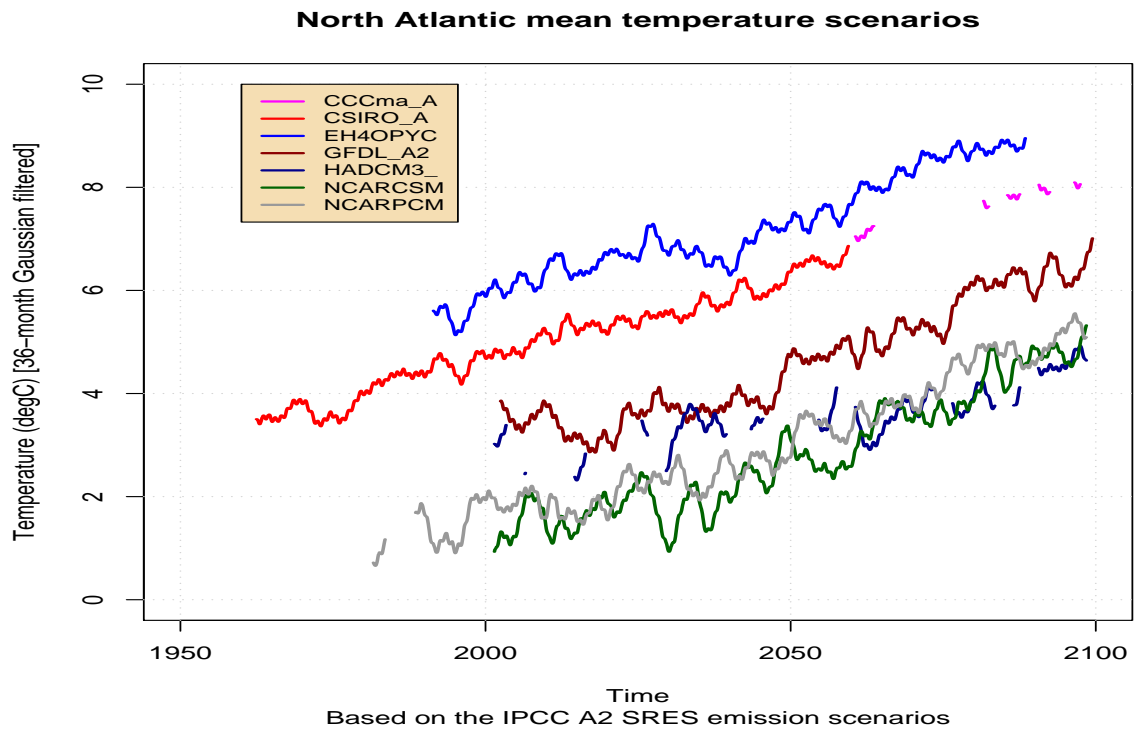
Figure 4. Comparison of the the mean 40°W–40°E, 45°N–85°N temperature computed by climate models following the IPCC a) B2 and b) A2 SRES scenarios.

North Atlantic mean precipitation scenarios

a

North Atlantic mean precipitation scenarios

b
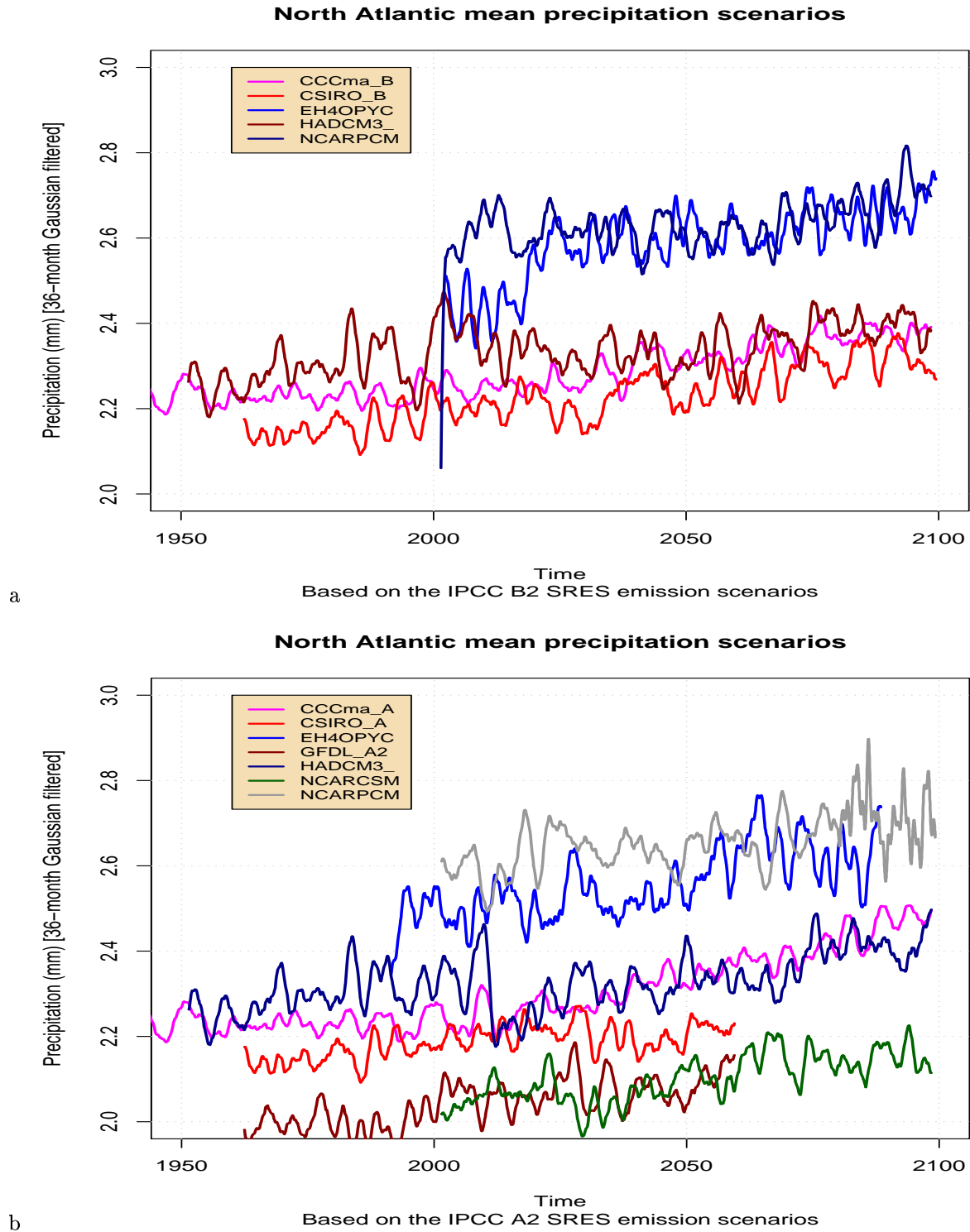
Figure 5. Comparison of the the mean 40°W–40°E, 45°N–85°N precipitation computed by climate models following the IPCC a) B2 and b) A2 SRES scenarios.

towards wetter conditions in the future. There are no clear differences between the A2 and B2 scenarios in these figures.

Figure 6 shows a comparison between the geographical distribution of the mean temperature from six different model integrations based on the IPCC B2 scenario. All the maps show similar spatial structures and similar values. A similar conclusion can be drawn for the model results from the A2 integrations (Figure 7). The maps in Figure 6 and 7 contain the same features as the the map based on the NCEP reanalysis (Figure 1a). Hence, all the models appear to reproduce the temperature in a realistic manner. A crude comparison with the results based on IPCC IS92a scenarios (*Benestad*, 2000) (using many of the same climate models) suggests an improved inter-model agreement on features such as the 0°C isoline in the Norwegian-Barents Sea region (Figure 1 in *Benestad* (2000)).

Figures 8–9 show maps of mean precipitation derived using the climate models following the B2 and A2 IPCC SRES scenarios respectively. In general, all the models predict most rainfall in the tropics, mainly in convergence zones such as the ITCZ and the SPCZ. A comparison with the NCEP results in Figure 1b suggests that the models capture the most important large-scale structure. However, the CCCma and GFDL results do not exhibit as well-defined ITCZ and CCCma reveals a feature similar to the SPCZ that extends northward instead of southward. The ECHAM4/OPYC3 and HadCM3 results suggests a more realistic spatial structure of the convergence zones, but much higher values in the Indian Ocean and the West Pacific compared to other regions (Note, the different scales in Figure 1b and in Figure 8–9 are due to different units: $Kg/m^2/s$ and mm/day respectively). The NCAR-PCM and NCAR-CSM results contain unrealistic features south of the equator in the Pacific that resemble an exaggeration of the southern branch of the ITCZ. The NCAR-PCM and NCAR-CSM models also appear to give higher rainfall amounts in the tropical regions than the other models.

Figures 10–11 show maps of the mean SLP field produced by the climate models. In general, these results are similar to the corresponding fields based on the NCEP reanalysis (Figure 1c). The greatest differences are in the Antarctic, where the observations are sparse. The mean SLP fields derived using the IPCC SRES scenarios are also similar to those based on the IPCC IS92a scenarios (Figure 5 in *Benestad* (2000)). Hence, the model reproduction of the mean SLP fields can be considered as realistic.

Figure 12 shows maps of mean temperatures and geopotential heights at different levels in the atmosphere and the specific humidity at 850hPa from the ECHAM4/OPYC3 B2 integration. Comparing the T(850hPa) temperatures in Figure 12 to those from the NCEP reanalysis (Figure 1d) suggests similar large-scale structures in general, albeit with some differences in the details. Hence, the T(850hPa) temperatures derived from ECHAM4/OPYC3 are realistic. The maps of specific humidity at 850hPa (Figure 12d and Figure 1e) suggest similar spatial large-scale structures, but differ in detail such as the contrasts between the values in the tropics and the high-latitudes (greater meridional gradient in ECHAM4/OPYC3). ECHAM4/OPYC3 does not produce a local maximum in q near the Himalayas. It it important to keep in mind the level of uncertainty associated with the humidity data in the NCEP reanalysis.

Figure 13 shows various mean fields from the HadCM3 B2 integration. A comparison between the 850hPa geopotential heights derived using the ECHAM4/OPYC3 (Figure 12f) and the HadCM3 (Figure 13a) suggests similar large-scale features, but also differences on the smaller scales. The regions of maxima are largely similar, but the 1350m and 1400m isolines exhibit some differences over the Newfoundland and the Labrador Sea region. These differences may have implications for the North Atlantic Storm Track. The differences in the corresponding mean SLP fields in Figures 10c–d suggest that the North Atlantic Storm Track may be less well-developed in the HadCM3, with a shorter extension into the Norwegian Sea. Figure 13b shows the relative humidity field* at 850hPa derived by the HadCM3 model. The lowest relative humidity is seen over the desert regions: the Sahara, the southwest U.S.A., west coasts of south America and south Africa, and Australia. The direct comparison between specific humidity† and relative humidity is not straight forward, when using monthly mean values, and such a comparison will not be made here. These two quantities are related, and it is nevertheless possible to identify similar regions of dry air in the specific humidity fields (Figure 12d and Figure 1e). The mean all-year snow-cover map shown in Figure 13c exhibit obvious differences to the snow-cover derived from the NCEP reanalysis (Figure 1f). Most of the snow in the HadCM3 B2 integration appears to have vanished, even around

---

*The amount of water vapor actually in the air divided by the amount of water vapor the air can hold.
†The mass of water vapor in a parcel divided by the total mass of the air in the parcel (including water vapor).
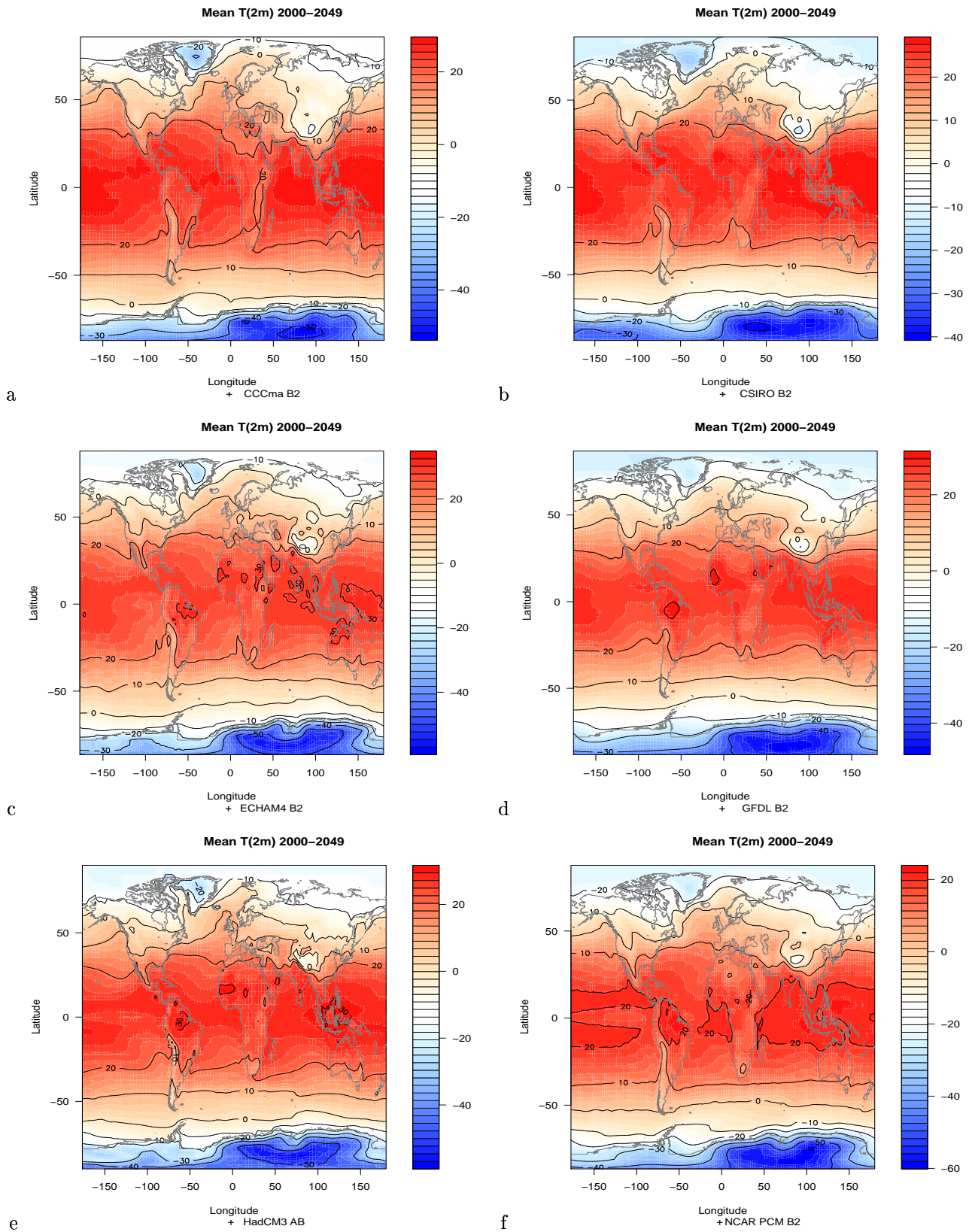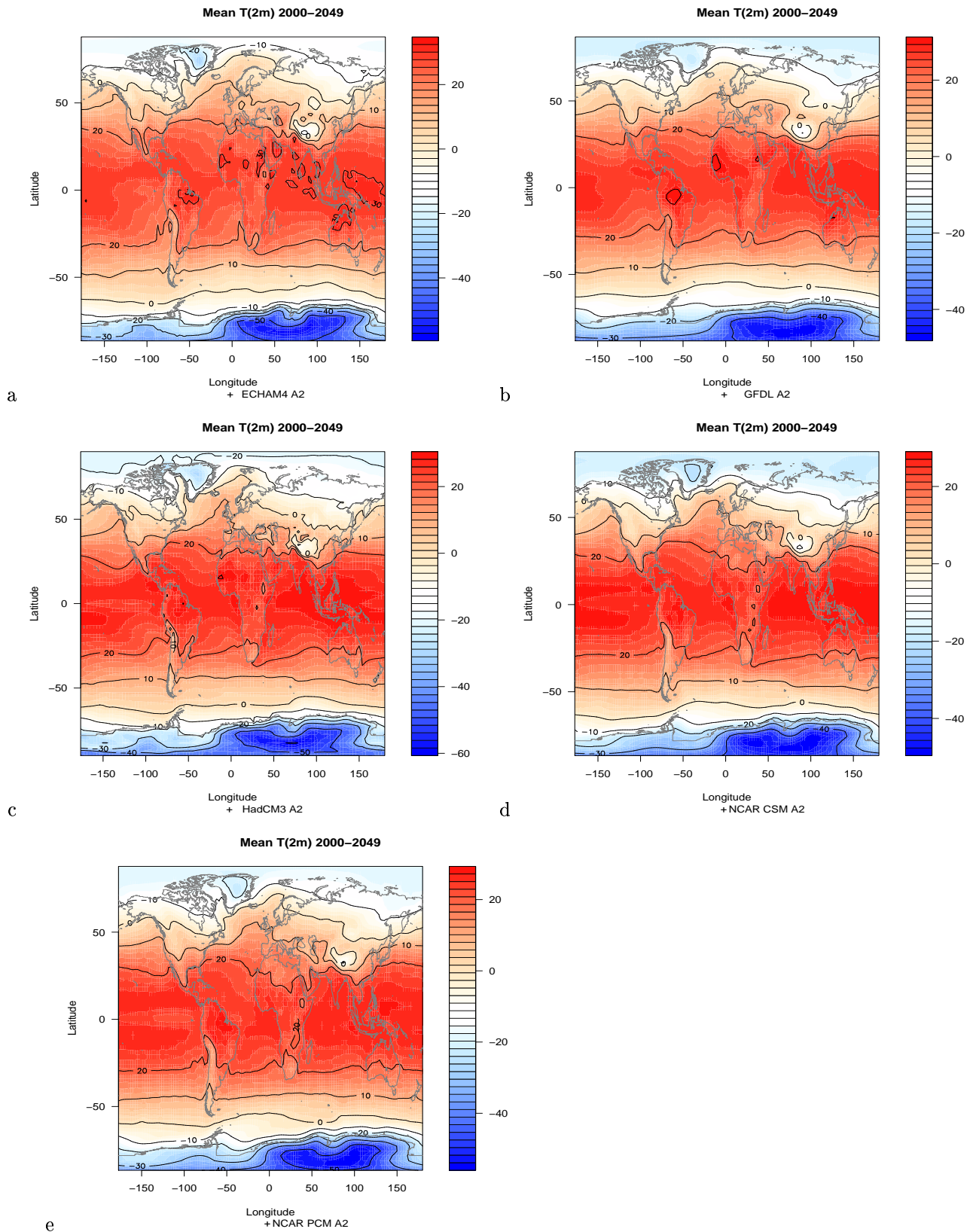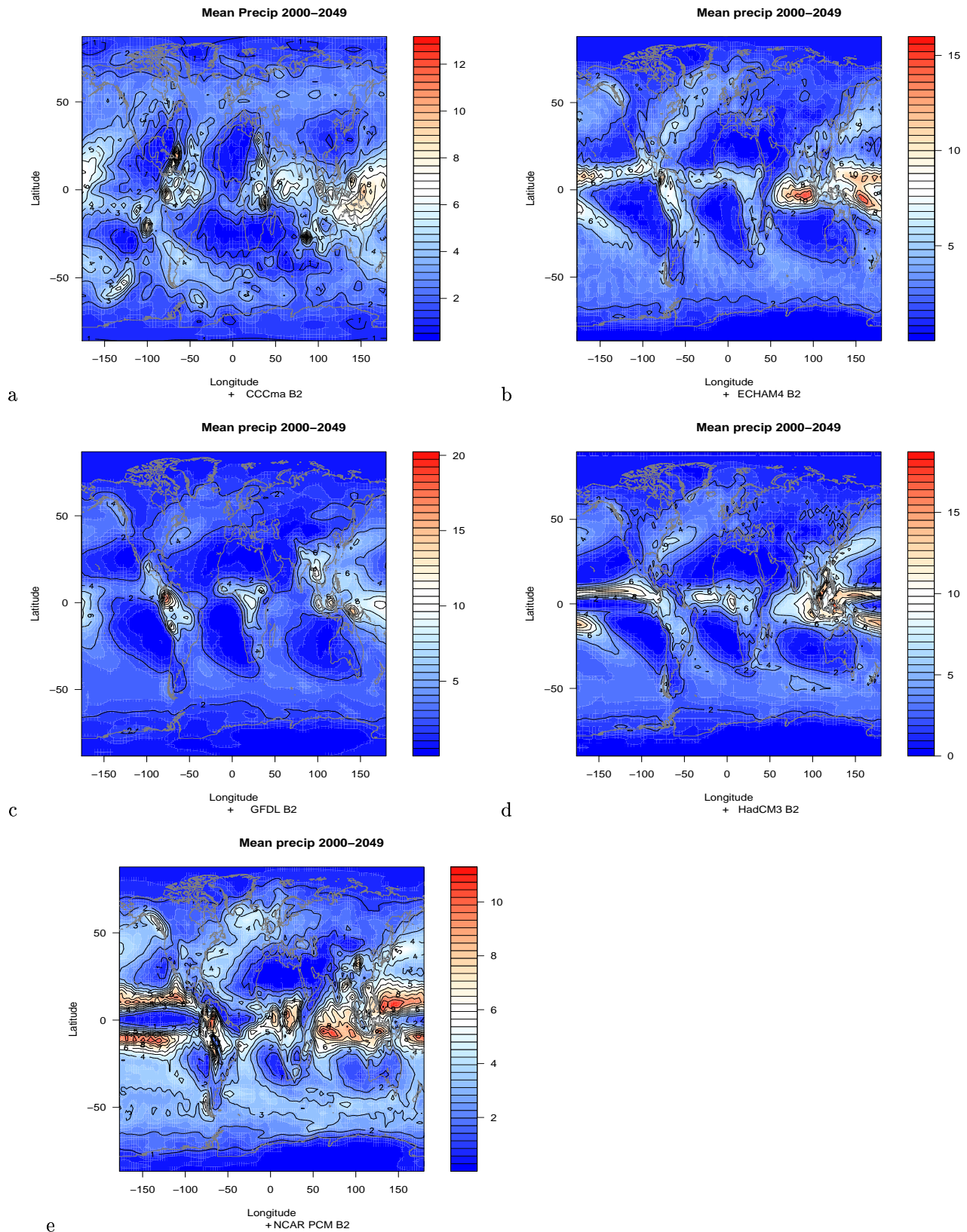
Figure 6.   Maps showing the geographical distribution of mean values for near-surface temperature computed by climate models following the IPCC B2 SRES scenario over "2000"–"2049" for the following models: a) CCCma, b) CSIRO, c) ECHAM4/OPYC3, d) GFDL-R30, e) HadCM3, f) NCAR-PCM.
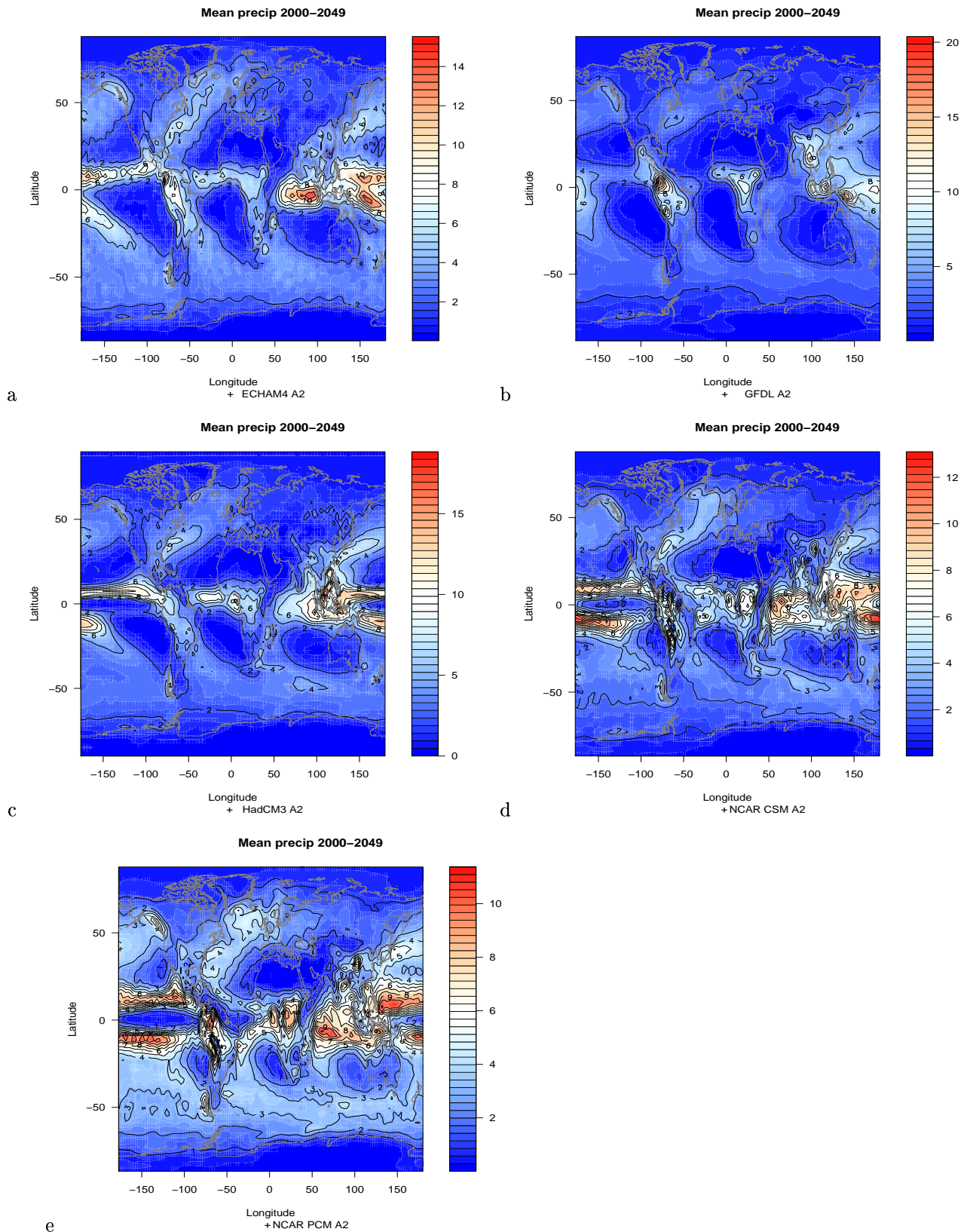
Figure 7. Maps showing the geographical distribution of mean values for near-surface temperature computed by climate models following the IPCC A2 SRES scenario over "2000"–"2049" for the following models: a) ECHAM4/OPYC3, b) GFDL-R30, c) HadCM3, d) NCAR-PCM, e) NCAR-CSM.
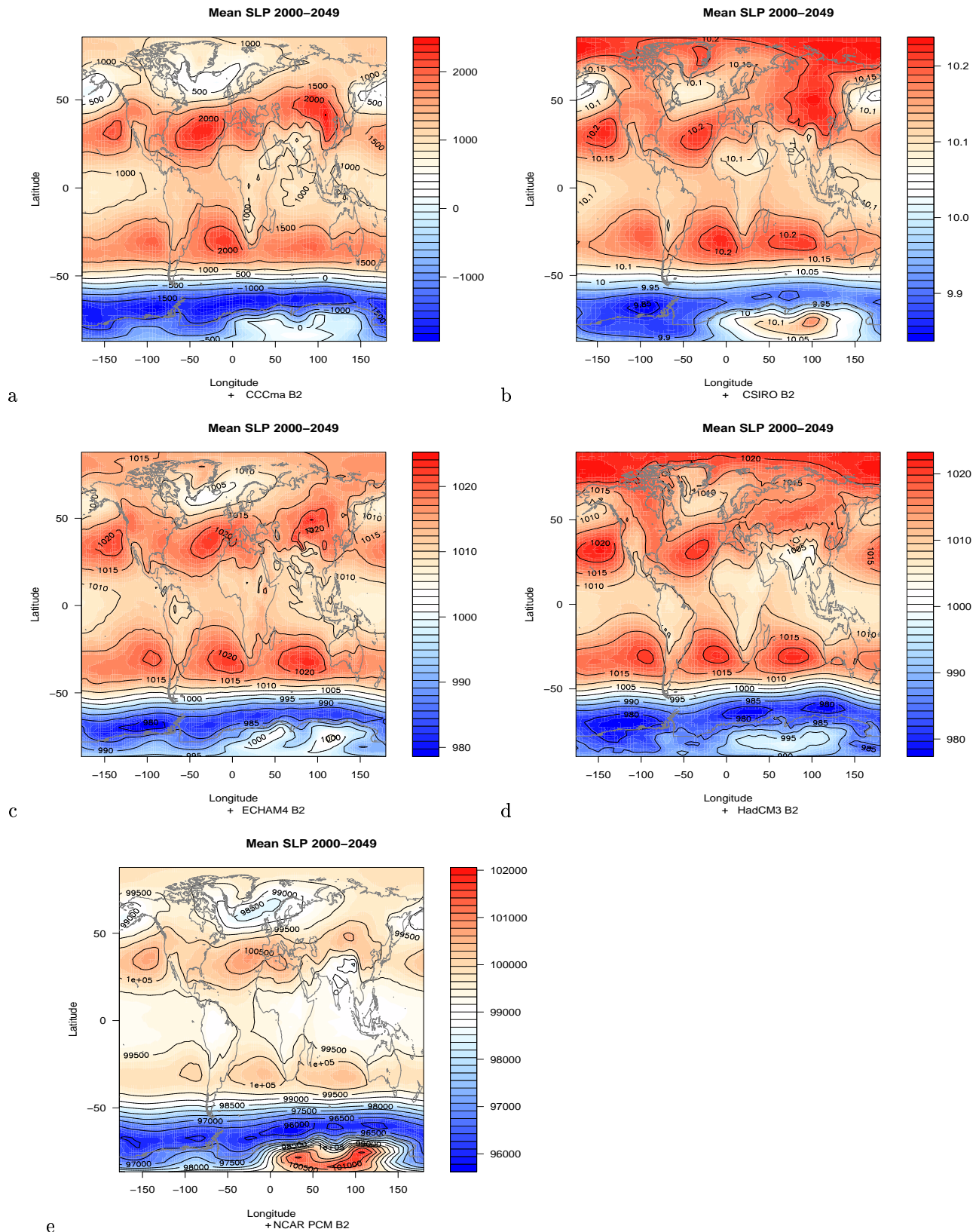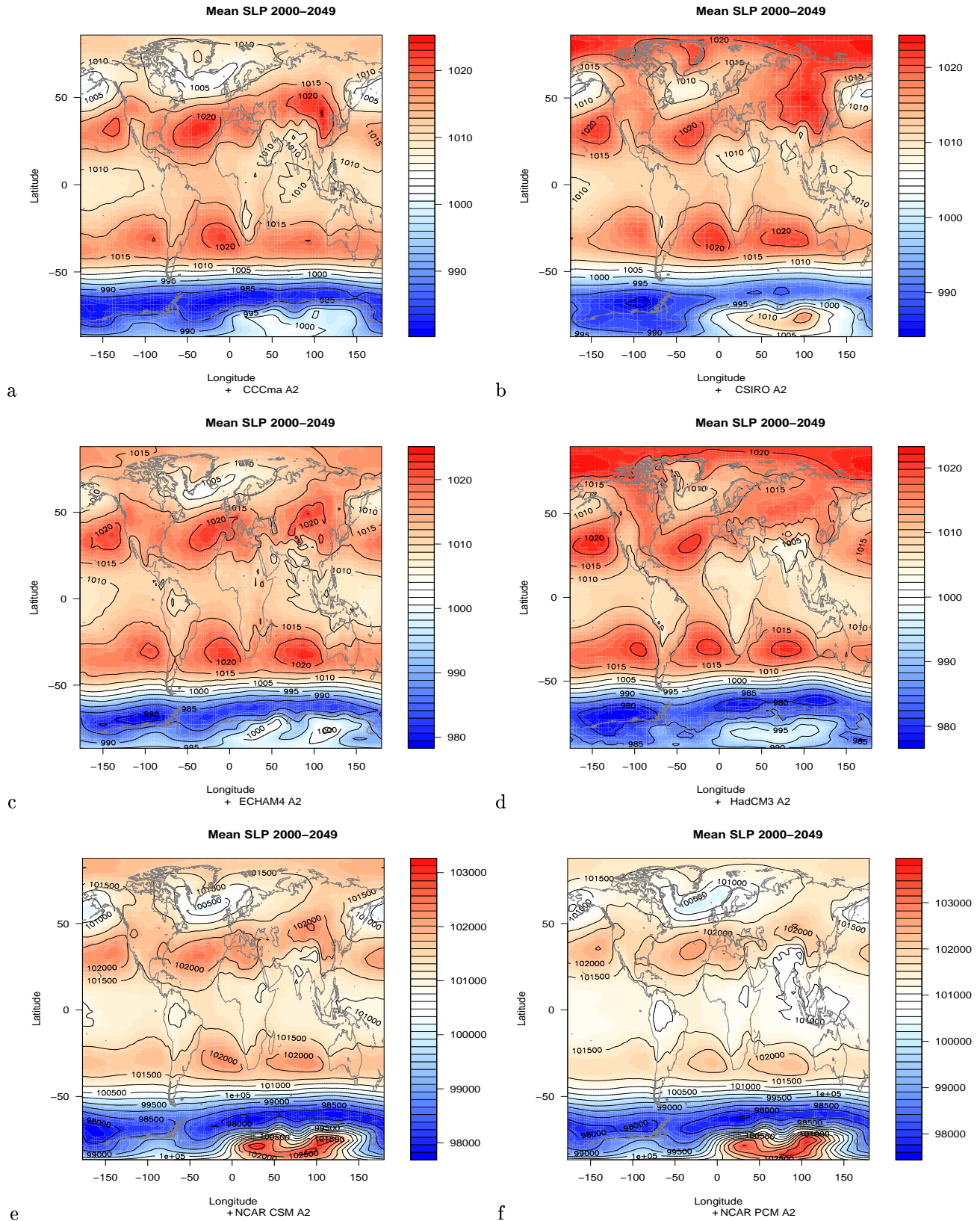
Figure 8.   Maps showing the geographical distribution of mean values for precipitation (unit: mm/day) computed by climate models following the IPCC B2 SRES scenario over "2000"–"2049" for the following models: a) CCCma, b) ECHAM4/OPYC3, c) GFDL-R30, d) HadCM3, e) NCAR-PCM.

Figure 9. Maps showing the geographical distribution of mean values for precipitation (unit: mm/day) computed by climate models following the IPCC A2 SRES scenario over "2000"–"2049" for the following models: a) ECHAM4/OPYC3, b) GFDL-R30, c) HadCM3, d) NCAR-PCM, e) NCAR-CSM.

Figure 10.   Maps showing the geographical distribution of mean values for sea level pressure computed by climate models following the IPCC B2 SRES scenario over "2000"–"2049" for the following models: a) CCCma, b) CSIRO, c) ECHAM4/OPYC3, d) HadCM3, e) NCAR-PCM.
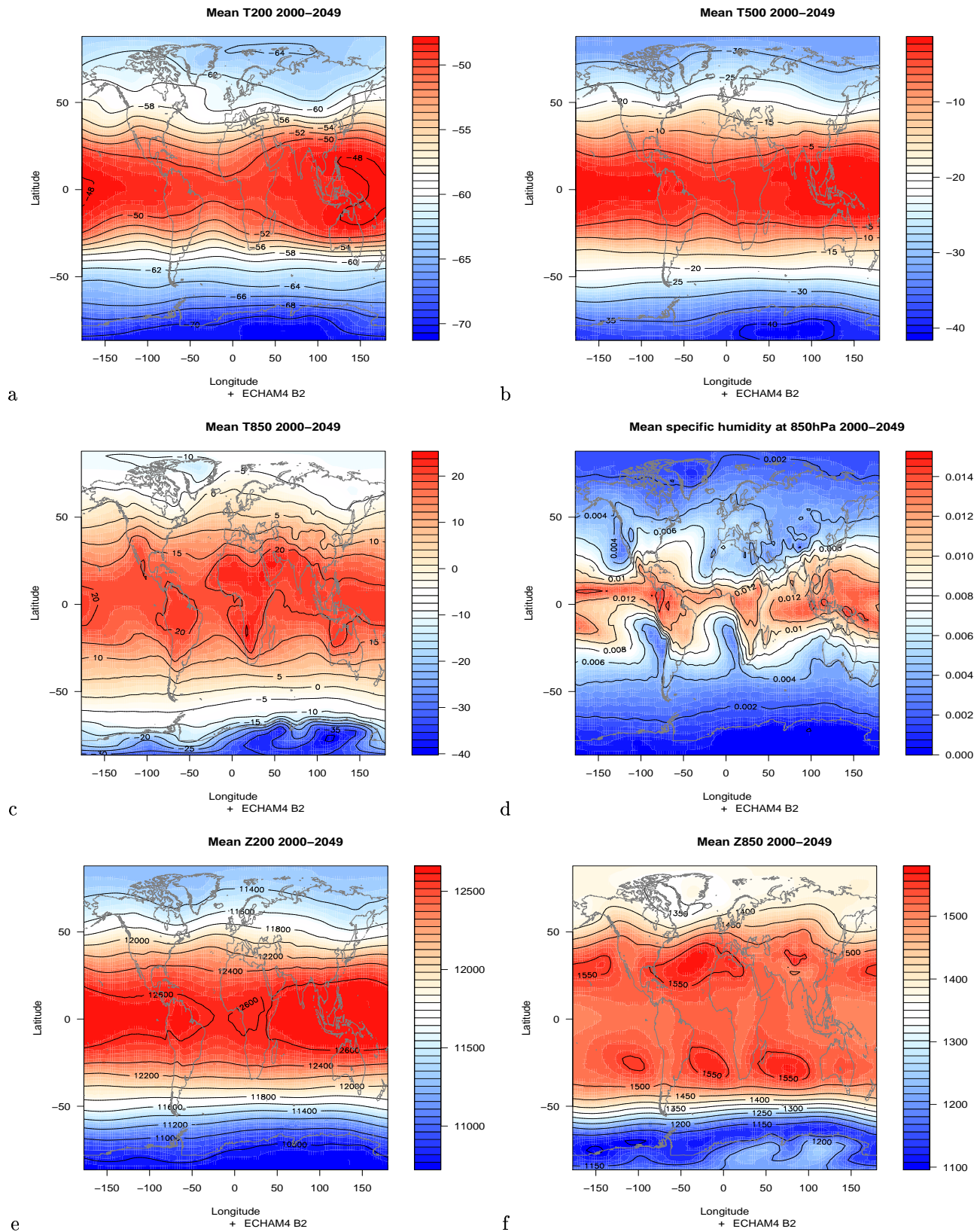
Figure 11. Maps showing the geographical distribution of mean values for near-surface temperature computed by climate models following the IPCC A2 SRES scenario over "2000"–"2049" for the following models: a) CCCma, b) CSIRO, c) ECHAM4/OPYC3, d) HadCM3, e) NCAR-PCM, f) NCAR-CSM.

Figure 12. Maps showing the geographical distribution of mean values for a) T(200hPa), b) T(500hPa), c) T(850hPa), d) specific humidity at 850hPa, geopotential heights at e) 200hPa and f) 850hPa computed by climate models following the IPCC B2 SRES scenario over "2000"–"2049" for ECHAM4/OPYC3.
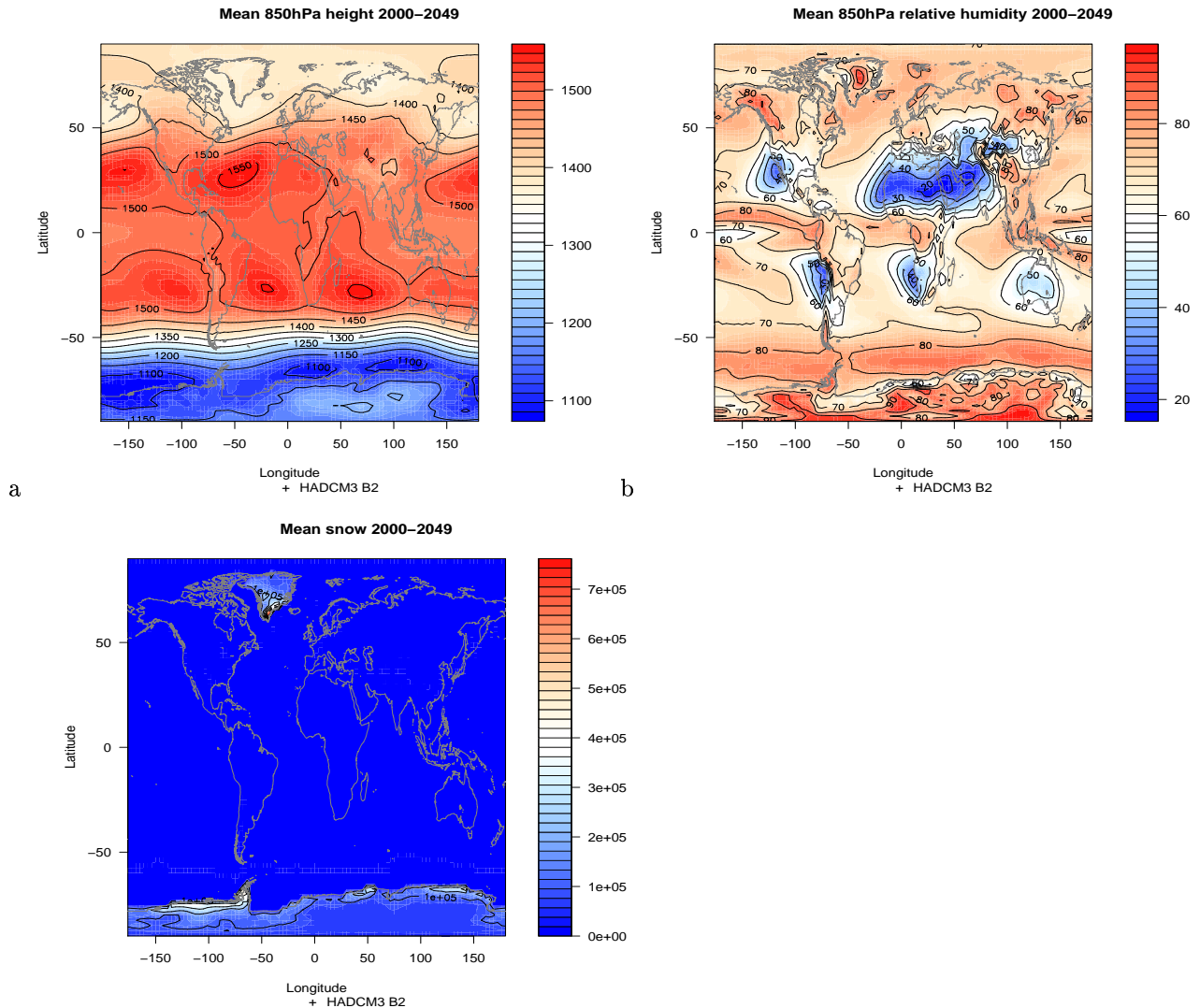
Figure 13. Maps showing the geographical distribution of mean values for a) geopotential heights at 850hPa, b) relative humidity at 850hPa, c) snow cover computed by climate models following the IPCC B2 SRES scenario over "2000"–"2049" for HadCM3.

year "2000", and this is clearly unrealistic.

3.2 A survey of trends

Figures 14–15 show various "2000"–"2049" trend statistics compiled from ensembles of model results based on the IPCC B2 and A2 SRES scenarios respectively. Panel a shows a measure of the model spread in terms of the inter-quantile range (IQR*). The greatest spread is seen in the high northern latitudes. The geographical distribution of the ensemble mean "2000"–"2049" trends is shown in panel b. The strongest warming appears to take place over the northern hemisphere continents and ice covered regions. The indication of weak warming over the Antarctic is surprising.

Panel c shows how the temperature trends depend on altitude (the altitude was derived from the topographical data shown as shading in panel b). The spread in trend estimates are generally greatest for altitudes less than 1000m a.s.l.. The CCSR/NIES tends to give stronger warming than the other models, and the CCSR/NIES can be regarded as an outlier in this respect. Some models give a negative
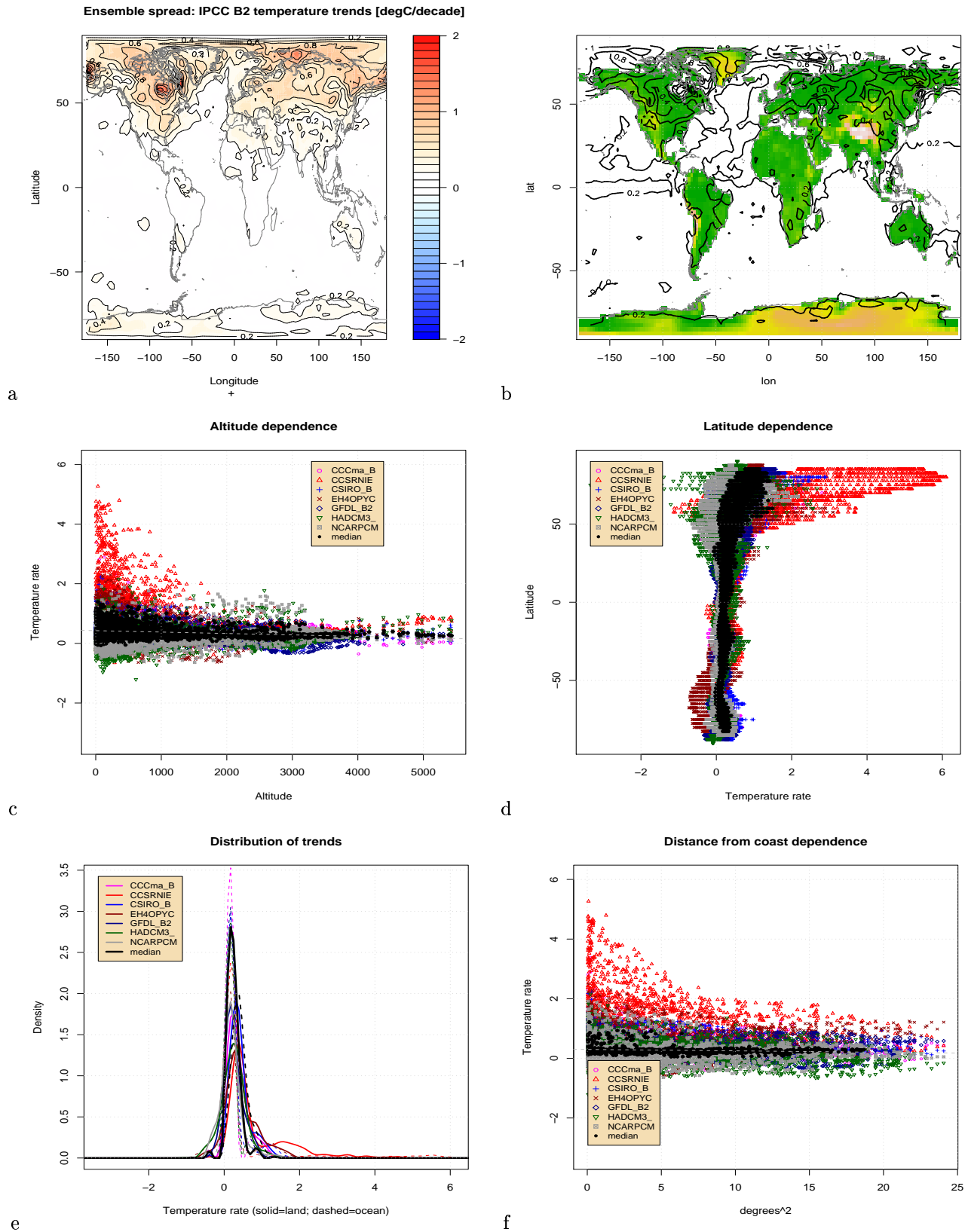
*IQR = the 75% percentile minus the 25% percentile.

Figure 14.   a) Maps showing the inter-quantile range of the trends in the "2000"–"2049" temperature (units: degree centigrade per decade) B2 SRES scenarios and b) the ensemble mean warming trend (contours) on top of the topography (shading). Panel c) shows the warming trend dependency on altitude, d) latitude, e) ocean-land, and f) distance from the coast (land points only). The models include: CCCma, CCSR/NIES, CSIRO, ECHAM4/OPYC3, GFDL, HadCM3, and NCAR-PCM.
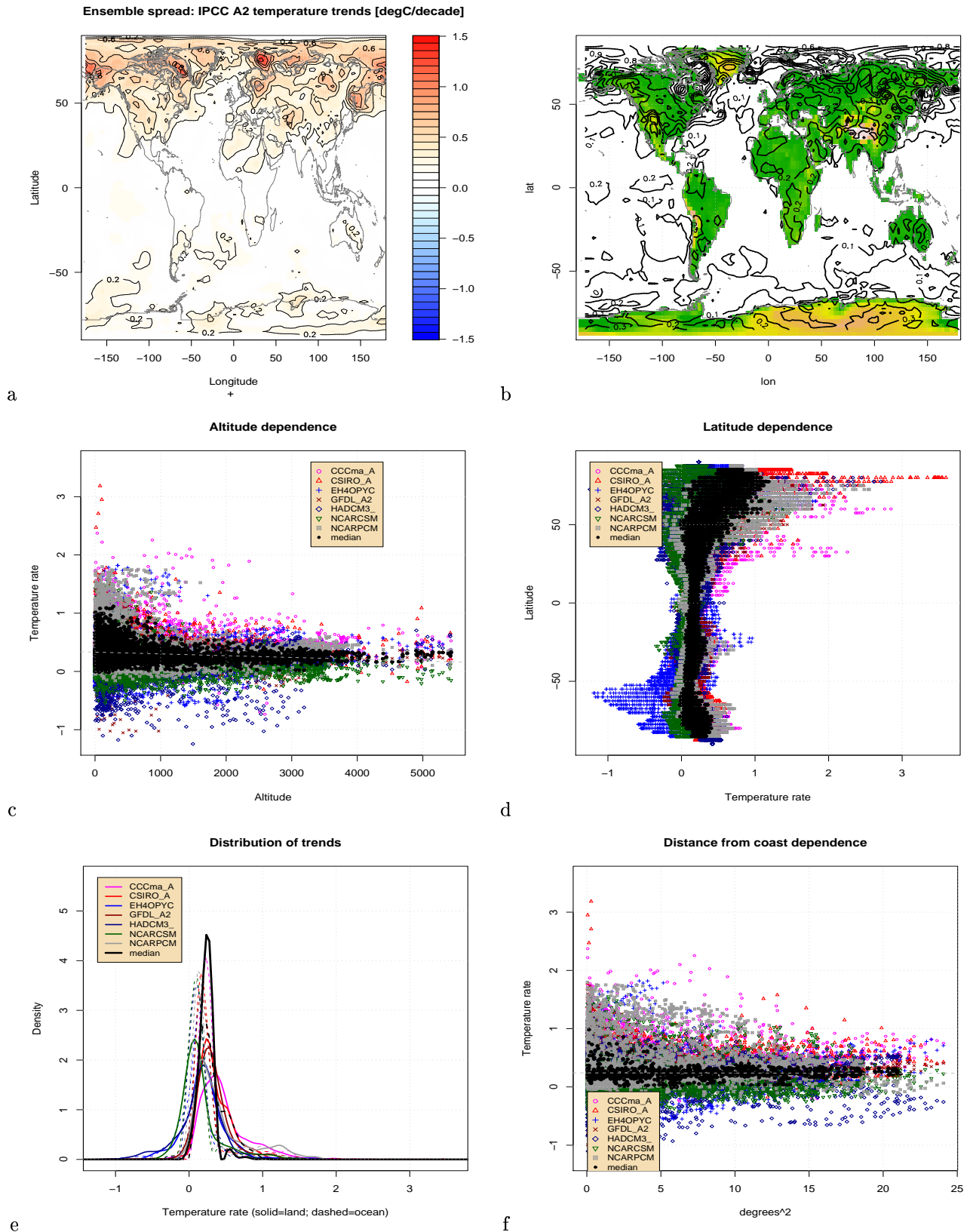
Figure 15. a) Maps showing the inter-quantile range of the trends in the "2000"–"2049" temperature (units: degree centigrade per decade) A2 SRES scenarios and b) the ensemble mean warming trend (contours) on top of the topography (shading). Panel c) shows the warming trend dependency on altitude, d) latitude, e) ocean-land, and f) distance from the coast (land points only).

trend in a few small regions in the B2 scenario. There is a clear systematic latitudinal dependency with faster warming in the high northern latitudes. Panel e shows the distribution of warming rates over land (solid) and ocean (dashed). In general, the models indicate similar ranges, with broader distributions for land than for ocean.

Figures 16–17 show show similar statistics as Figures 14–15, but now for precipitation. The largest model spread and strongest trends are found in the tropics. The spread in trend estimates also have a clear latitudinal dependency, with the greatest scatter at low altitudes (near the coasts, also see panel f). The distribution of the trend magnitudes are largely similar for land and ocean regions, however, the distributions over the ocean tend to have a fatter upper tail, suggesting slightly more rapid increase in the rainfall.

4   Discussion and conclusion

climate model data from integrations following the IPCC B2 and A2 SRES scenarios have been retrieved from the IPCC data distribution Internet site, and then converted from the GRIB format to netCDF. A first-order quality control has been carried out. The results from this evaluation suggest that the model data are sound after a couple of minor bugs have been corrected. A inter-model comparison suggest a high degree of similarity amongst various climate models, and a crude comparison with similar evaluation carried out on the IPCC IS92a scenarios hint to a closer agreement amongst the new SRES scenarios. One improvement of the recent SRES-based climate simulations over the older IS92a scenarios is the improvement in the climate models' general spatial resolution.

The conclusion from the report is that the climate model output are sufficiently realistic and are appropriate for the use in climate studies and empirical downscaling.
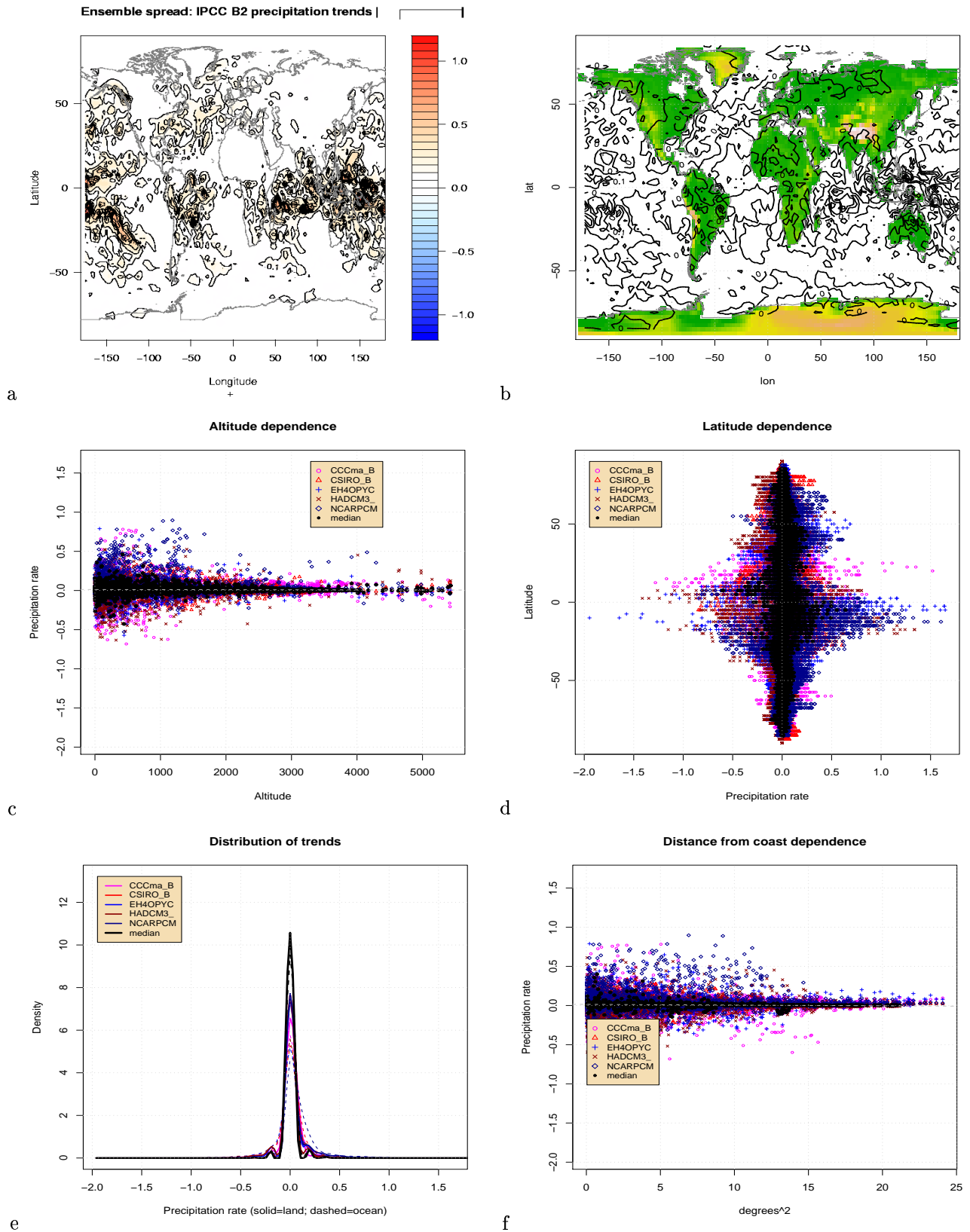
Figure 16. a) Maps showing the inter-quantile range of the trends in the "2000"–"2049" precipitation (in units mm/day/decade) B2 SRES scenarios and b) the ensemble mean trend (contours) on top of the topography (shading). Panel c) shows the trend dependency on altitude, d) latitude, e) ocean-land, and f) distance from the coast (land points only).

a

b

c

d

e

f

Figure 17.   a) Maps showing the inter-quantile range of the trends in the "2000"–"2049" precipitation (in units mm/day/decade) A2 SRES scenarios and b) the ensemble mean trend (contours) on top of the topography (shading). Panel c) shows the trend dependency on altitude, d) latitude, e) ocean-land, and f) distance from the coast (land points only).
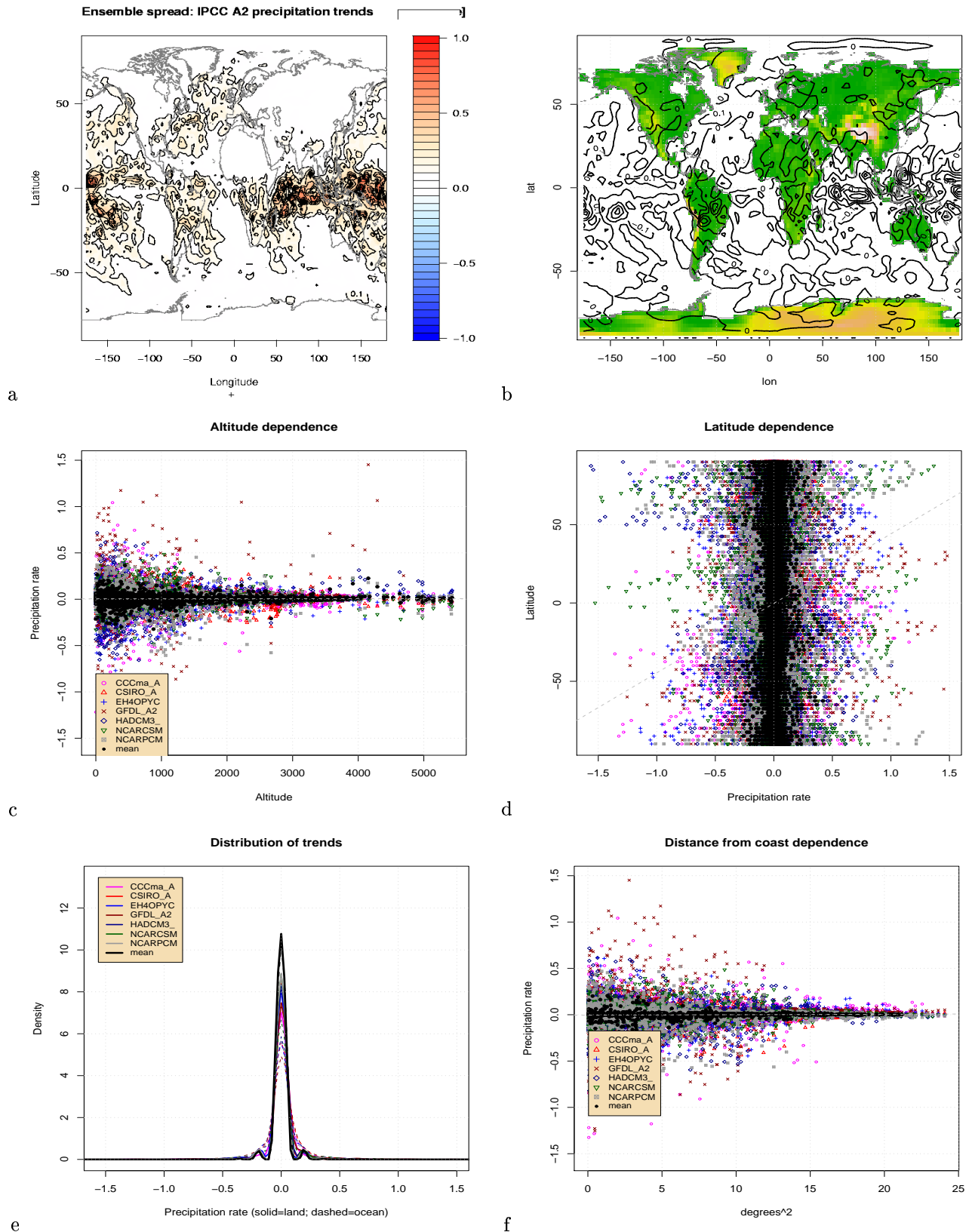
References

Benestad, R.E., 2000. *Fifteen Global Climate Scenarios: The conversion to netCDF and quality control.* KLIMA 16/00. DNMI, PO Box 43 Blindern, 0313 Oslo, Norway.

Benestad, R.E., 2003. *Downscaling analysis for daily and monthly values using clim.pact-V.0.9.* KLIMA 01/03. met.no, PO Box 43 Blindern, 0313 Oslo, Norway.

Ellner, Stephen P., 2001. Review of R, Version 1.1.1. *Bulletin of the Ecological Society of America,* **82**(2), 127–128.

Gentleman, R., & Ihaka, R., 2000. Lexical Scope and Statistical Computing. *Journal of Computational and Graphical Statistics,* **9**, 491–508.

Houghton, J.T., Ding, Y., Griggs, D.J., Noguer, M., van der Linden, P.J., Dai, X., Maskell, K., & Johnson, C.A., 2001. *Climate Change 2001: The Scientific Basis.* Contribution of Working Group I to the Third Assessment Report of IPCC. International Panel on Climate Change, (Available from www.ipcc.ch).

Kalnay, E., Kanamitsu, M., Kistler, R., Collins, W., Deaven, D., Gandin, L., Iredell, M., Saha, S., White, G., Wollen, J., Zhu, Y., Chelliah, M., Ebisuzaki, W., Higgins, W., Janowiak, J., Mo, K.C., Ropelewski, C., Wang, J., Leetmaa, A., Reynolds, R., Jenne, R., & Joseph, D., 1996. The NCEP/NCAR 40-Year Reanalysis Project. *Bull. Amer. Meteor. Soc.,* **77**(3), 437–471.